Donepezil-based hybrids as multifunctional anti-Alzheimer's disease chelating agents: Effect of positional isomerization

Marina Costa, [a)] Romane Josselin,[a)] Diana F. Silva, [b)] Sandra M. Cardoso, [b),c)] Nóra V. May, [d)] Sílvia Chaves, [a)*] M. Amélia Santos [a)*]

[a)] *Centro de Quimica Estrutural, Instituto Superior Tecnico, Universidade de Lisboa, Av, Rovisco Pais 1, 1049-001, Lisboa, Portugal*
[b)] *CNC – Center for Neuroscience and Cell Biology, University of Coimbra, Coimbra, Portugal*
[c)] *Institute of Molecular and Cell Biology, Faculty of Medicine, University of Coimbra, Coimbra, Portugal*
[d)] *Research Centre for Natural Sciences, 1117 Magyar tudósok körútja 2 Budapest, Hungary*

Keywords: Hydroxyphenyl-benzimidazole; Donepezil; Anti-neurodegeneratives; Alzheimer´s disease; Multifunctional drugs; Metal chelation.

* Corresponding authors:

(Sílvia Chaves) E-mail: silvia.chaves@tecnico.ulisboa.pt; Phone: +351-218419269

(M. Amélia Santos) E-mail: masantos@tecnico.ulisboa.pt; Phone: +351-218419273

Abstract

The intricate and multifactorial nature of Alzheimer´s disease (AD) requires the development of compounds able to hit different pathophysiological targets, such as cholinergic dysfunction, deposits of amyloid-β peptide (Aβ) and metal dyshomeostasis. In order to continue the search for new anti-AD drugs, a design strategy was followed based on repositioning donepezil (DNP), by attaching a benzylpiperidine mimetic of DNP moiety at different (ortho, para) attachment points of a hydroxyphenyl-benzimidazole (BIM) chelating unit. Herein, two compounds (**1** and **2**) are compared in terms of their potential multiple properties: both present good AChE inhibition (low micromolar range) and are moderate/good inhibitors of A*β* self- and Cu-mediated aggregation; although compound **1** has a higher chelating capacity towards Cu^{2+} (pCu = 14.3, pZn = 6.4, pH 7.4, C_L/C_M = 10, $C_M = 10^{-6}$ M) than **2** (pCu = 10.7, pZn = 6.3), attributed to its ability to establish a tridentate (N,O,O) coordination to the metal ion. Both compounds are eligible as drug candidates for oral administration but compound 1 shows improved neuroprotective role by completely preventing Aβ-induced cell toxicity.

1. Introduction

Alzheimer's disease (AD) is one of the most common and devastating age-dependent neurodegenerative disorders and its prevalence is expected to enormously increase in the coming years because of the population growth and ageing [1]. Hence, there has been a worldwide intensive research aimed to understand and find treatment for AD, but no cure has been found so far [2,3]. Currently approved AD therapeutics are only able to attenuate the dementia symptoms by compensating the cholinergic deficit, as the acetylcholinesterase (AChE) inhibitors (tacrine, donepezil, rivastigmine, galantamine) or the glutamate N-methyl D-aspartate (NMDA) receptor antagonist (memantine) [4].

The recognized multifactorial nature and consequent complexity of AD are believed to account for the absence of disease-modifying drugs. In fact, the formation of misfolded protein aggregates, namely β-amyloid (Aβ) plaques (a prominent hallmark of AD), dyshomeostasis of metal ions and oxidative stress are among the many factors that are implicated in the trigger and progression of AD [5]. Furthermore, although Aβ imbalance has been considered to be a causative agent in AD, high levels of metals (e.g. Fe, Cu, Zn) have been found in the Aβ plaques of AD brains and, in particular, Cu and Zn bind to Aβ peptides, promoting their aggregation, while redox active metal ions (e.g.

Cu, Fe) promote overproduction of reactive oxygen species (ROS) that can damage biomolecules [6–8]. Therefore, to address the multiple pathological factors and their potential interconnections in AD pathogenesis, in the last decade there has been a change of paradigm from singletarget drugs towards multi-target drugs as chemical entities (the so called multi-target ligands) able to address multiple biological targets involved in the disease, aimed to get possible therapeutic answers [9–11].

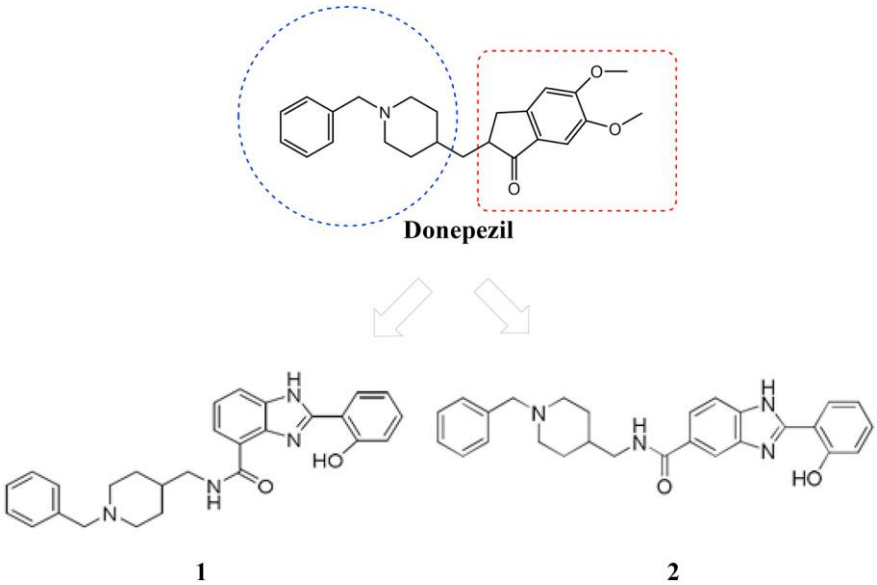

Fig 1. DNP and DNP-BIM hybrids (1 and 2), chelators with different attachment points between the benzylpiperidine and the BIM moieties.

In recent years, several research groups, including ours, have developed hybrid compounds, via a rational structure-based methodology which integrates a moiety with capacity for AChE inhibition with a framework able to interact with Aβ and also possess metal cheating capacity, so that to associate the symptom treatment with disease modifying roles, namely to inhibit the Aβ self- and metal-induced aggregation and to attenuate the metal-promoted ROS formation [12–16]. Herein we report the synthesis, physico-chemical and biological evaluation as well as molecular modeling of a new donepezil-hydroxyphenylbenzimidazole (DNP-BIM) chelating hybrid (1) (Fig. 1). This compound results from a structural modification of a recently reported positional isomer DNP hybrid (2) [17], for the sake of increasing ligand denticity and thus improving the metal chelating capacity as well as the control/modulation of interconnected multiple pathological features of AD, namely those that could arise from the synergy of its metal chelation and Aβ interaction properties.

2. Experimental

2.1. *Chemistry*

2.1.1. *General methods and materials*

Analytical grade reagents were purchased and used as supplied. Solvents were dried according to standard methods [1]. The chemical reactions were monitored by TLC using alumina plates coated with silica gel 60 F_{254} (Merck). Column chromatography separations were performed on silica gel Merck 230-400 mesh (Geduran Si 60). The melting points (m.p.) were measured with a Leica Galen III hot stage apparatus and are uncorrected. The ^{1}H- and ^{13}C-NMR spectra were recorded on Bruker AVANCE III spectrometers at 300 and 400 MHz, respectively. Chemical shifts (δ) are reported in ppm from the standard internal reference tetramethylsilane (TMS). The following abbreviations are used: s = singlet, d = doublet, t = triplet, m = multiplet. Mass spectra (ESI-MS) were performed on a 500 MS LC Ion Trap (Varian Inc., Palo Alto, CA, USA) mass spectrometer equipped with an ESI ion source, operated in the positive or negative ion mode. For the target compounds, the elemental analyses were performed on a Fisons EA1108 CHNS/O instrument at LAIST and were within the limit of ± 0.4%. The electronic spectra were recorded with a Perkin Elmer Lambda 35 spectrophotometer, using thermostated 1-cm path length cells and the fluorescence measurements were performed with a Spectramax Gemini EM (Molecular Devices) fluorimeter.

2.1.2. Synthesis of compound **1**

2.1.2.1. *2-((1-Benzylpiperidin-4-yl)methyl)isoindoline-1,3-dione (1a)*

Phthalic acid anhydride (1 eq) and 4-(aminomethyl)piperidine (1 eq) were heated at 160 °C for 4 h. The resulting dark brown solid was mixed with K_2CO_3 (6.6 eq), triethylamine (1.4 eq) and benzyl chloride (2.3 eq) and refluxed in acetonitrile for 3 h. Then, the mixture was cooled at rt, added to water, and extracted with ethyl acetate (three times). The organic layers were collected, dried over sodium sulphate anhydrous, and concentrated under reduced pressure. The crude was purified through chromatography column (eluent: ACN/H_2O/NH_4OH 92:8:0.1), affording a white solid (η = 29%); M.P. = 130 °C. ^{1}H NMR (300 MHz, MeOD-d_4), δ (ppm): 1.37 (m, 2H, *Pip*), 1.67 (d, 2H, J = 12.0 Hz, *Pip*), 1.80 (m, 1H, *Pip*), 2.02 (td, 2H, J = 12.0 Hz, *Pip*), 2.91 (d, 2H, J = 12.0 Hz, *Pip*), 3.51 (s, 2H, NCH_2Ph), 3.58 (d, 2H, J = 12.0 Hz, NCH_2CH), 7.34-7.29 (m, 5H, *Ph*), 7.89-7.79 (m, 4H, *Phth*); m/z (ESI-MS): 335.00 $(M+H)^+$.

2.1.2.2. ***(1-Benzylpiperidin-4-yl)methanamine (1b)***

2-((1-Benzylpiperidin-4-yl)methyl)isoindoline-1,3-dione (1 eq) and hydrazine monohydrate (6 eq) were dissolved in absolute ethanol and warmed at 60 °C for 3 h. The reaction mixture was then filtered and concentrated under reduced pressure. The residue was dissolved in dichloromethane, washed with brine (three times), dried over anhydrous sodium sulphate, and concentrated under reduced pressure obtaining a pure yellow-orange oil (η = 30.5%). ^{1}H NMR (300 MHz, MeOD-d_4), δ (ppm): 1.01-1.21 (m, 2H, *Pip*), 1.64 (d, 2H, *J* = 12.0 Hz, *Pip*), 1.86 (t, 1H, *J* = 12.0 Hz, *Pip*), 2.40 (d, 2H, *J* = 12.0 Hz, *Pip*), 2.78 (d, 2H, *J* = 12.0 Hz, NCH_2CH) 2.91 (d, 2H, *J* = 12.0 Hz, *Pip*), 3.51 (s, 2H, NCH_2Ph), 7.34-7.19 (m, 5H, *Ph*)

2.1.2.3. ***2-(2-Hydroxyphenyl)-1H-benzo[d]imidazole-4-carboxylic acid (1c)***

To a solution of salicylaldehyde (1 eq) and $Na_2S_2O_5$ (1.2 eq) in the green solvent (glycerol/choline chloride (2:1)) was added the 2,3-diaminobenzoic acid (1 eq). The mixture was heated at 50 °C for 30 min. Then, the mixture was cooled at rt, added to water and filtrated. The afforded solid was washed with water and then dichloromethane and then purified by recristallisation in EtOAc and MeOH. The title compound was obtained as a purple solid (η =25.2%), m.p. >300°C. ^{1}H NMR (300 MHz, MeOD-d_4), δ (ppm): 7.08 (d, 2H, *J* = 8.0 Hz, *BIM*); 7.42 (m, 2H, *J* = 8.0 Hz, *BIM*), 7.96 (t, 2H, *J* = 8.0 Hz, *BIM*), 8.25 (d, 1H, *BIM*); m/z (ESI-MS): 253 (M-1)+, 255.00 (M+1)+.

2.1.2.3. ***N-((1-benzylpiperidin-4-yl)methyl)-2-(2-hydroxyphenyl)-1H-benzo[d]imidazole-4-carboxamide (1)***

To a solution of the 2-(2-hydroxyphenyl)-1H-benzo[*d*]imidazole-4-carboxylic acid (1 eq, **1c**) and (1-benzylpiperidin-4-yl)methanamine (1 eq, **2b**), in dry DMF, was added *N*-hydroxysuccinimide (1 eq) and DCC (1 eq), and the reaction mixture was left stirring for 24 h at r.t.. Then the precipitate obtained (urea) was filtered off and the liquid phase was diluted with ethyl acetate and washed with brine (3 times), dried over anhydrous sodium sulfate, concentrated under reduced pressure and purified by recrystallization in EtOAc affording a yellow solid (η = 24.2%); m.p. = 192-193 °C. ^{1}H RMN (300 MHz, MeOD-d_4), δ (ppm): 1.75-1.95 (m, 5H, *Pip*), 2.17 (t, 2H, *J* = 12 Hz, *Pip*), 3.02 (d, 2H, *J* = 12 Hz, *Pip*), 3.49 (d, 2H, *J* = 6 Hz, CH_2NCO), 3.60 (s, 2H, CH_2Ph), 7.00-7.08 (m, 2H, *Ph*), 7.28-7.42 (m, 7H, *Ph*), 7.79 (d, 1H, *J* = 9 Hz, *BIM*), 7.89 (d, 1H, *J* = 8 Hz, *BIM*), 8.16 (d, 1H, *J* = 9 Hz, *BIM*). ^{13}C RMN (100 MHz, MeOD-d_4), δ (ppm): 29.25, 33.35, 44.31, 52.77, 62.44, 116.65, 119.45, 119.54, 122.13, 127.18, 127.59, 127.84, 129.50, 129.59, 131.84,

131.91, 135.91, 136.56, 139.11, 139.33, 151.40, 157.44, 161.38; m/z (ESI-MS): 439.00 (M-1), 441.00 (M+1).

2.2. Molecular modeling for ligand-AChE docking

To perform the ligand-enzyme docking studies, the X-ray crystallographic structure of *Torpedo californica*-AChE (*Tc*AChE) complexed with an inhibitor (donepezil, Dnp) was taken from RCSB Protein Data Bank (PDB entry 1 EVE) [2], in order to be used as enzyme model. This structure was chosen because of the similarity between the original inhibitor (DNP) and ligands **1** and **2**, namely relatively to the benzylpiperidine moieties. The original structure was treated using Maestro v. 9.3 [3] by removing the original ligand, solvent, and co-crystallization molecules, and then adding the hydrogen atoms. The ligands were built using Maestro, and then, using Ghemical v. 2.0 [4], they were submitted to random conformational search (RCS) of 1000 cycles, and 2500 optimization steps using Tripos 5.2 force field [5]. The minimized ligands were docked into the AChE structure with GOLD software v. 5.1 [6], and the zone of interest was defined as the residues within 10 Å from the original position of the ligand in the crystal structure. The 'allow early termination' option was deactivated and the remaining default parameters of Gold were used. The ligands were subjected to 100 genetic algorithm steps using ASP as fitness function.

2.3. Prediction of pharmacokinetic properties

To analyze the drug like behavior of the DNP-BIM hybrids, the prediction of their main pharmacokinetic properties was performed *in silico*. This procedure determined parameters such as the lipo-hydrophilic character (*c*log *P*), blood–brain barrier partition coefficient (log BB), the ability to be absorbed through the intestinal tract (Caco-2 cell permeability) and CNS activity.

The ligands were built and minimized as previously mentioned for the docking studies. The structures were submitted to the calculation of these relevant pharmacokinetic properties and descriptors using QikProp v. 2.5 [7]. These predictions are for orally delivered drugs and assume non-active transport.

2.4. Metal chelation studies

2.4.1. *Potentiometric and UV-vis spectrophotometric titrations*

Solutions. The aqueous copper ($CuCl_2$, 0.015 M) and zinc ($ZnCl_2$, 0.0156 M) stock solutions for potentiometric and spectrophotometric equilibrium studies were prepared from 1000 ppm standards (Titrisol) and their metal content was evaluated by atomic absorption. The titrant solution (0.1 M KOH) was obtained from a carbonate-free commercial concentrate (Titrisol) and standardized by potentiometric titration with potassium hydrogen phthalate. The titrant solution was discarded whenever the percentage of carbonate (Gran's method) [8] was about 0.5% of the total amount of base.

Measurements. Compound **1** was titrated in 50% (w/w) DMSO/H_2O medium, at $T = 25.0 \pm 0.1$ °C and ionic strength (I) 0.1 M KCl, by using 0.1 M KOH as titrant. Both glass and Ag/AgCl reference electrodes were previously conditioned in DMSO/H_2O mixtures with increasing amount of DMSO and the response of the glass electrode was controlled by strong acid – strong base (HCl/KOH) calibrations with the determination of the Nernst parameters by Gran's method [8]. The measurements were performed in a final volume of 30.00 mL, with the ligand concentrations (C_L) 6.7×10^{-4} M (potentiometry) and 4.0×10^{-5} M (spectrophotometry), under different C_M/C_L ratios: 0:1 (L), 1:1 and 1:2 (M = Cu, Zn). The spectrophotometric measurements were carried out at pH ca 2.5-11.5, in the 300–420 nm wavelength range. All titrations were performed in duplicate and under the stated experimental conditions the pK_w value (13.6) was determined and subsequently used in the computations. The stepwise protonation constant of the ligand, $K_i = [H_iL]/[H_{i-1}L][H]$, and the overall metal–complex stability constants, $\beta_{M_mH_hL_l} = [M_mH_hL_l]/[M]^m[H]^h[L]^l$, were calculated by fitting the potentiometric and spectrophotometric data with, respectively, Hyperquad 2008 [9] and PSEQUAD programs [10]. The metal hydrolysis constants were determined under the defined experimental conditions (I = 0.1 M KCl, 50% w/w DMSO/H_2O, T = 25.0 ± 0.1 °C) and the following values of stability constants were included in the fitting of experimental data towards the equilibrium models related to the Cu^{2+}/L and Zn^{2+}/L systems: log $\beta_{Cu_2H_{-2}}$ = -9.99; log β_{ZnH-2}= -14.79, log β_{ZnH-3} = -23.48. Species distribution curves were plotted with the Hyss program [9].

2.4.2. *ESI-MS spectra*

The pH of the Cu(II)/**1** ($C_L = 2.25 \times 10^{-4}$ M) and Zn(II)/**1** ($C_L = 2.25 \times 10^{-4}$ M) systems in 50% w/w DMSO/water medium was previously ascertained to 4.28 (C_L/C_{Cu} = 1) and 6.42 (C_L/C_{Cu} = 2), as well as to 7.01 and 8.39 (C_L/C_{Zn} = 2), by using KOH solution, and the respective mass spectra were obtained from a LCQ Fleet mass spectrometer operated

in the ESI positive and negative ion mode (Thermo Scientific). The optimized parameters were as following: ion spray voltage, +4.5/-2.5 kV; capillary voltage, 16/-28 V; tube lens offset, -63 V; sheath gas (N_2), 80 arbitrary units; auxiliary gas, 5 arbitrary units; capillary temperature, 250 °C. The spectra were recorded in the range 100 – 1000 Da. Spectra typically correspond to the average of 20–35 scans.

2.4.3. *EPR spectra*

CW-EPR spectra were recorded with a BRUKER EleXsys E500 spectrometer (microwave frequency 9.85 GHz, microwave power 10 mW, modulation amplitude 5 G, modulation frequency 100 kHz). Two samples were prepared for each compound (**1** and **2)**, one at ligand excess and another around equimolar concentration in 50% w/w DMSO/water solution. The pH of the Cu(II)/**1** (C_L = 1.48 × 10^{-3} M) system was ascertained to 6.75 (C_L/C_{Cu} = 1) and 6.91 (C_L/C_{Cu} = 1.5), while that of the Cu(II)/**2** (C_L = 2.23 × 10^{-3} M) system was to 5.46 (C_L/C_{Cu} = 1) and 5.72 (C_L/C_{Cu} = 2), by using KOH solution. Room temperature spectra were measured in capillary at 298 K. Anisotropic EPR spectra were recorded in quartz EPR tubes immersed in a Dewar containing liquid nitrogen (77 K); 0.025 mL MeOH was added to the 0.2 mL sample to avoid water crystallization upon freezing. All recorded EPR spectra, and anisotropic EPR spectra at 77 K, were simulated by the EPR program [11]. To describe the isotropic spectra the parameters g_0, A_0^{Cu} copper hyperfine ($\boldsymbol{I_{Cu}}$= 3/2) and $\boldsymbol{a_0^N}$ nitrogen ($\boldsymbol{I_N}$ = 1) superhyperfine couplings have been taking into account. The four copper(II) linewidths were treated with individual linewidth parameters. The g-tensor (g_x, g_y, g_z), copper hyperfine tensor $(A_x^{Cu}, A_y^{Cu}, A_z^{Cu})$ and nitrogen hyperfine tensor $(a_x^N, a_y^N, a_z^N$, for wich x y and z denotes the directions of the g-tensor) parameters were fitted. For the description of the linewidth the orientation dependent α, β and γ parameters were used to set up each component spectra. Since a natural copper(II)chloride was used for the measurements, both the isotropic and anisotropic spectra were calculated as the sum of the spectra of ^{63}Cu and ^{65}Cu weighted by their natural abundances. The hyperfine and super-hyperfine coupling constants and the relaxation parameters were obtained in field units (Gauss = 10^{-4} T).

2.4.4. *Molecular modeling of the copper complexes*

In the absence of X-ray structure, a molecular modelling study was performed aimed at providing some further insight into the 1:1 (M/L) copper complex structures of compounds **1** and **2**, considering, respectively, one and two water molecules in the

coordination shell. These studies were carried out with full geometry optimization of the Cu(II) complexes by quantum mechanical calculations based on DFT methods included in the Gaussian 03 program software [12] with the B3PW91 hybrid functional. Preliminary molecular simulation was obtained by using 3-21G basis set and afterwards 6-31G**. No symmetry constrains were enforced during geometry optimization with the two basis sets. The calculations were performed as well for one water molecule by using the B3PW91 functional, first with the 3-21G basis set and subsequently re-optimized via 6-31G** basis set. Frequency calculations were performed to confirm the nature of the minima. The electronic energies (E_{b1}) obtained at the PBE0/b1 level of theory were converted to free energy (G_{b1}) at 298.15 K and 1 atm by using zero point energy and thermal energy corrections based on structural and vibration frequency data calculated at the same level.

2.5. *Biological studies*

2.5.1. *Acetylcholinesterase inhibition*

The enzymatic activity of AChE was determined using an adaptation of Ellman's method, as already described [13,14]. Firstly, a stock solution of AChE was prepared by dissolving enzyme 500 U in 10 mL of tris(hydroxymethyl)aminomethane (TRIS) buffer (50 mM, pH 8). Then, 4-(2-hydroxyethyl)-1-piperazineethanesulfonic acid (HEPES) buffer was used for further dilution of the enzyme solution therefore obtaining the final working solution of AChE. The assay solution consisted of 374 μL of HEPES buffer (50 mM and pH 8.0), a variable volume (10–50 μL) of the compound's stock solution (1 mg/mL of MeOH), 476 μL of 3 mM bis(3-carboxy-4-nitrophenyl) disulfide (DTNB), 25 μL of AChE stock solution and the necessary amount of methanol to attain the same volume of sample mixture in a 1 mL cuvette. After mixing, samples were left to incubate for 15 min and then 75 μL of 16 mM acetylthiocholine iodide (AChI) solution was added and immediately the reaction was monitored at 405 nm for 5 min. Firstly, enzyme activity was determined by measuring the rate of enzymatic reaction in solution by recording absorbance (with or without enzyme) at 405 nm. To calculate the percent inhibition of AChE, the enzyme activity in the presence of increasing concentrations of the test compound, as well as for a blank reaction (methanol without compounds), were measured at 405 nm.

The obtained results were expressed in percentage of inhibition through the Eq. (1):

$$\% I = 100-(v_I / v_0 \text{ x } 100) \quad (1)$$

Where v_I is the initial reaction rate in the presence of the inhibitor and v_0 is the initial rate of the control reaction. The curves of inhibition were obtained using a plot of percentage of enzymatic inhibition versus inhibitor concentration, and a calibration curve was obtained from which the linear regression parameters were obtained.

2.5.2. *Inhibition of self- and Cu^{2+}-mediated Aβ aggregation*

Amongst the methods used to measure the aggregation of $A\beta_{1-42}$, the assay based on Thioflavin T (ThT) is the standard procedure [15,16]. This test is performed with $A\beta_{1-42}$ peptide previously prepared by dissolving it in 1,1,1,3,3,3–hexafluoro-2-propanol (HFIP), an organic solvent useful to solubilize and monomerize the β–sheet protein aggregates and reserve them in the fridge. Films are re-dissolved in an Eppendorf tube with a fresh solution of a mixture of $CH_3CN/Na_2CO_3/NaOH$, to have a stable stock solution, and, afterwards, added to an optimized fibrillation phosphate buffer. The samples must be prepared using MeOH (1 mg/mL) as a solvent with the specific procedure, followed by incubation in a water bath for 24 h at 37°C with gentle shaking. After incubation, the samples were added to a 96-well plate (BD Falcon) with 180 µL of 5 µM ThT in 50 mM glycine-NaOH (pH 8.5) buffer. Blank samples were prepared for each concentration in a similar way, devoid of peptide. After 5-min incubation with the dye, the ThT fluorescence was measured at 446 nm (excitation) and 485 nm (emission).

2.5.3. *Cell viability and neuroprotection*

SH-SY5Y human neuroblastoma cell line (ATCC-CRL-2266) is grown in Dulbecco's modified Eagle's medium (DMEM), and were obtained from Gibco-Invitrogen (Life Technologies Ltd, UK) with 10% heat inactivated fetal calf serum, containing 50 U/mL penicillin and 50 µg/mL streptomycin, under a humidified atmosphere of 95% air- 5% CO_2 at 37 ºC. Cells were plated at 0.12×10^6 cells/mL for cell viability assay. The tested compounds were dissolved in DMSO at a concentration of 50 mM and aliquots were stored at -20 °C. We performed a dose-response screening (from 10 µM to 40 µM) in order to choose the highest non-toxic concentration. As a result we selected: 20 µM final concentrations for compounds **18, 19, 20** and **23**; 20 µM final concentrations for compound **19**; 35 µM final concentration for compounds **21** and **24**. The final concentration of DMSO in culture media did not exceed 0.05% (v/v) and no alterations on cells were observed. The compounds were added to the cell media 1 h before the

incubation with $A\beta_{1-42}$ or L-ascorbic acid/ferrous sulfate. $A\beta_{1-42}$ or L-ascorbic acid/ferrous sulfate where incubated alone or with the compound for an additional 24 h. $A\beta_{1-42}$ was prepared as 276.9 μM stock in sterile water and added to the medium at 2.5 μM final concentration. Ferrous sulfate was freshly prepared as 0.36 M stock in water and added to the medium at 500 μM final concentration. *L*-Ascorbic Acid was freshly prepared as 80 mM stock in water and added to the medium at 5 mM final concentration. $A\beta_{1-42}$ was purchased from Bachem (Torrance, CA, USA) and ferrous sulfate and L-ascorbic acid from Sigma Chemical Co (St. Louis, MO, USA).

Cell viability was determined by the MTT (3-(4,5-dimethylthiazol-2-yl)-2,5-diphenyltetrazolium bromide) reduction test. In viable cells, the enzyme succinate dehydrogenase metabolizes MTT into a formazan that absorbs light at 570 nm. Following the cell treatment protocol, the medium was aspirated and 0.5 mL MTT (0.5 mg/mL) was added to each well. The plate was then incubated at 37 °C for 1 h 30 min protected from light. At the end of the incubation period, the formazan precipitates were solubilized with 0.5 ml of acidic isopropanol (0.04 M HCl/isopropanol). The absorbance was measured at 570 nm [17]. Cell reduction ability was expressed as a percentage of untreated control cells.

All data were expressed as mean ±S.E.M. of at least three independent experiments performed in duplicates. Statistical analyses were performed using GraphPad Prism 5 (GraphPad Software, San Diego, CA, USA). Differences between two datasets were evaluated by two-tailed unpaired Student's t test A P – value < 0.05 was considered statistically significant.

3. Results and Discussion

*3.1. Synthesis of compound **1***

The synthesis of compound **1** involved the synthetic strategy summarized in Scheme 1, while the synthesis of compound 2 was previously reported [20].

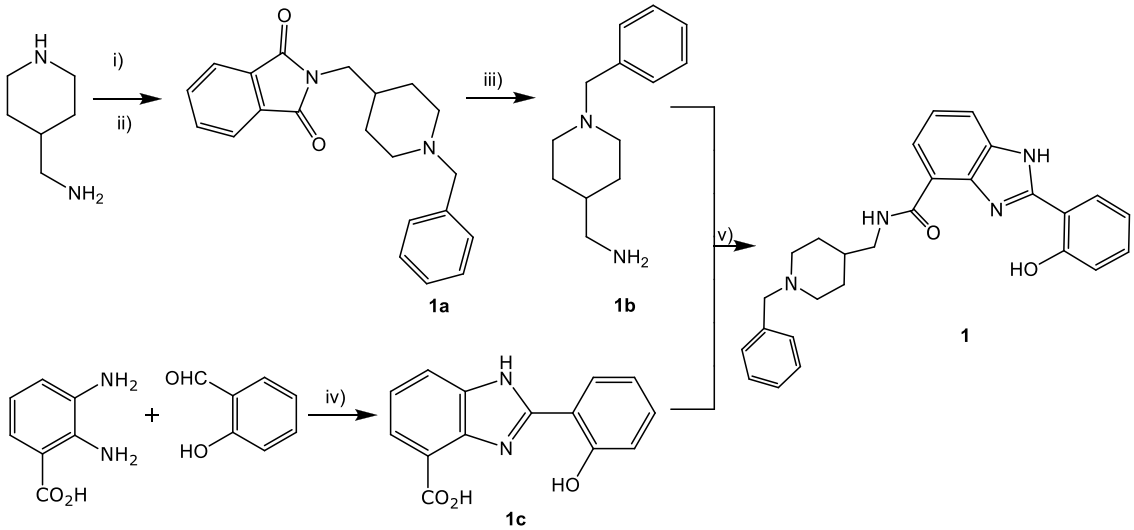

Scheme 1. Reagents and conditions**:** i) phthalic anhydride, 160 °C, 4 h; ii)) benzyl bromide, K_2CO_3, triethylamine, acetonitrile, 50 °C, 3 h; (iii) N_2H_4 xH_2O, absolute ethanol, reflux, 3 h, then RT, overnight; iv) dimethylacetamide, $Na_2S_2O_5$, 100°C, 12 h; v) DCC, *N*-hydroxysuccinimide, dry DMF, RT, 24 h.

This involved the synthesis of two main frameworks, a benzyl-piperidine-methanamine (**1b**) and carboxylic derivative of benzimidazole (**1c**), as well as their attachment through an amidic linkage. The preparation of **1b** involved a 3-step reaction. Firstly, the the primary amine group of the commercially available piperidinemethanamine was protected, as a phthalimide group, by reaction with phthalic anhydride, followed by the piperidine *N*-benzylation, by reaction with benzyl bromide in basic conditions, affording **1a.** This was subsequently released from phthalimide group by reaction with hydrazine hydrate in absolute ethanol, affording the free amine derivative (**1b**). Parallely, The hydroxyphenylbenzimidazole carboxylic acid (**1c**) was prepared by Mannich reaction between 3,4-diamino benzoic acid and salicylaldehyde and cyclization in the presence of the reducing agent sodium metabissulfite [19]. Finally the intermediates **1b** and **1c** were coupled to each other via amide bond formation, affording the novel hybrid **1**. This reaction was carried out in dry DMF with NHS and DCC as activators, under N_2 atmosphere for two days.

3.2. Molecular design and modeling studies of ligand-AChE interactions

DNP is undoubtedly a contemporary choice as anti-AD drug and therefore it was herein used as an inspiration to design the new hybrid 1. In this way, N-benzylpiperidine was enclosed in the structure of the hybrid and further connected to a hydroxyphenyl-benzimidazole (BIM) unit. The N-benzylpiperidine portion mimics the binding interaction of DNP within the catalytic anionic site (CAS) of AChE [12] while the BIM

moiety is expected to mimic the indanone segment of DNP in its interaction with the peripheral anionic site (PAS) of the enzyme, besides providing additional properties to the hybrids, such as anti-Aβ42 aggregation and metal chelating activity [16,17,40,41]. It is well known that DNP establishes a strong interaction within the active site of human acetylcholine esterase, hAChE, and also of the electric ray homologue (Torpedo californica), TcAChE. Notwithstanding some differences between the respective inhibitor-enzyme complexes, both enzymes are fairly conservative in terms of the main aminoacid residues that coat the active site gorge [42] and so the herein described modeling study was performed with TcAChE.

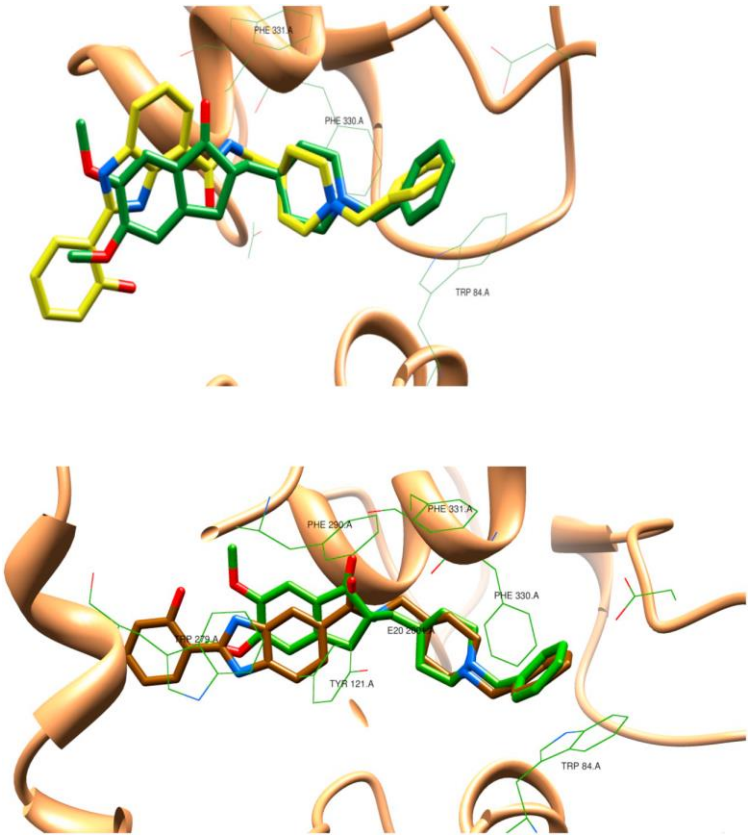

Fig. 2. Superposition of compound 1 (above) and 2 [17] (below) and the original ligand (DNP), from PDB code 1EVE, inside the TcAChE active site: DNP (green), compound 1 (yellow) and compound 2 (brown).

The binding of DNP to TcAChE includes three types of interactions: in the bottom of the gorge, the benzyl group establishes a parallel π-π stacking with the indole group of Trp84; in the middle of the gorge, the charged nitrogen atom can establish a cation-π binding interaction with the phenyl group of Phe330; at the entrance of the gorge, the indanone ring interacts through π-π stacking with the peripheral anionic residue Trp279. The

docking simulations with compounds 1 and 2 show some differences in their accommodation inside the gorge of the enzyme, namely concerning the interaction of the benzylpiperidine moiety with the aminoacid residues of CAS: in the case of compound 2 there is an excellent superimposition with the original ligand (DNP), while compound 1, thought it can establish identical binding through the piperidine nitrogen atom, it slightly deviates from the position of the original ligand (see Fig. 2). On the other way, the BIM moieties of both compounds seem to be involved quite similarly in the interactions with PAS, allowing a π-π interaction with the indole group from Trp279, although probably with a less favorable orientation than DNP. This fact is eventually due to the larger size of the BIM unit when compared with that of the indanone group of DNP. Therefore, as a conclusion, the modeling studies seem to predict that the ortho compound 1 is a less good AChE inhibitor than its positional isomer (compound 2).

3.3. *Acid-base properties*

The chelating capacity of compound **1**, with the BIM unit *ortho*-attached to the benzylpiperazinic moiety, was studied by pH-potentiometric (M = Cu^{2+}, Zn^{2+}) as well as ultraviolet-visible (UV-vis in the case of Cu^{2+} system) spectrophotometric titrations for the different M/L systems: 0:1, 1:1 and 1:2. A 50% w/w DMSO/water medium was adopted to perform these studies, due to some solubility problems of the compound. Nevertheless, in terms of cellular studies, the amount of ligand used is lower (< 7 μM) and so the final concentration of DMSO employed in culture media would be even inferior (< 1%), therefore not expecting to involve modifications in biological tissues.

In order to establish the metal chelating model, first the protonation constants of **1** were determined by both above referred experimental techniques (see **Fig. 1**) and the values obtained are contained in **Table 1**.

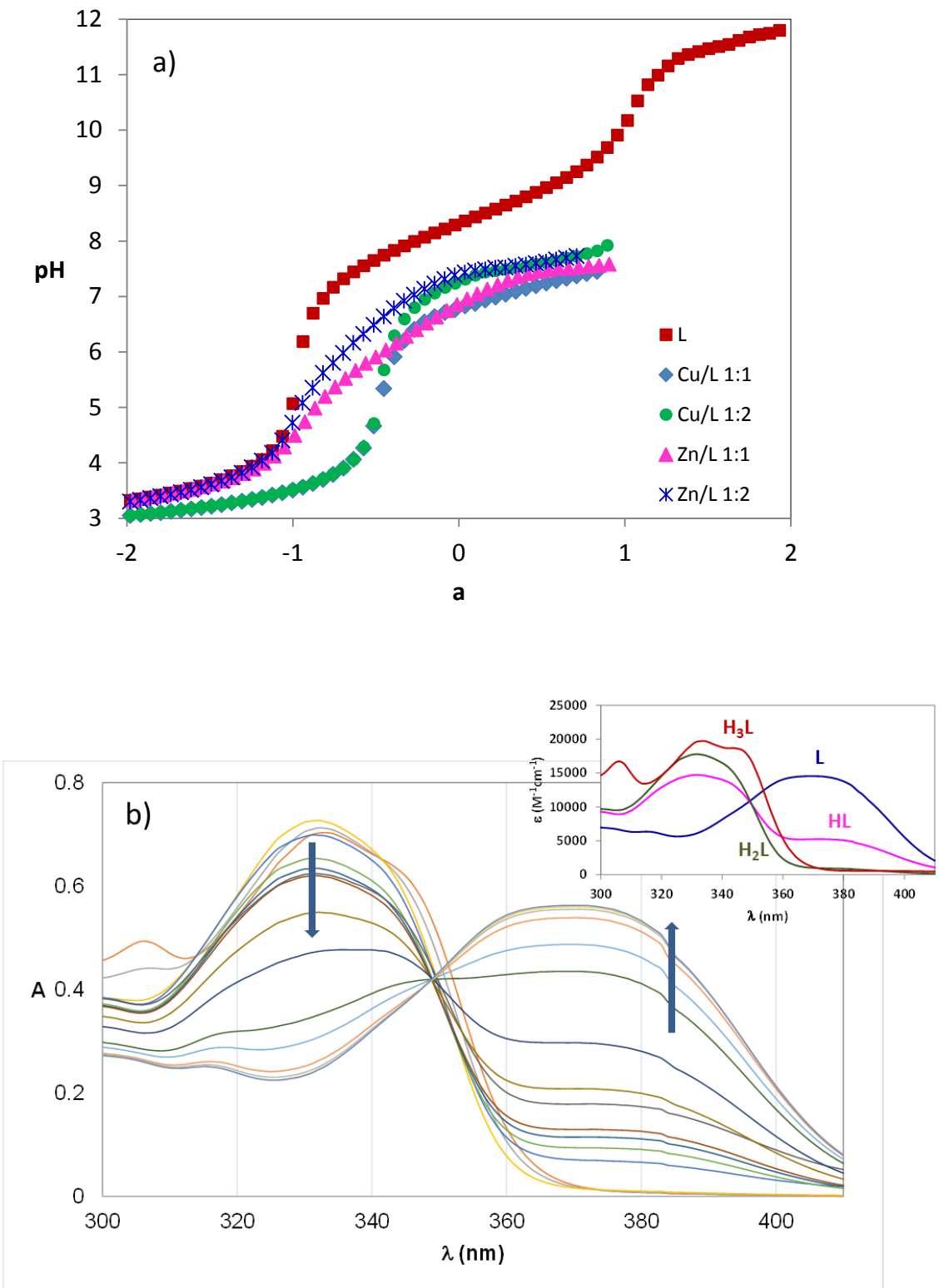

Figure 1 – a) Potenciometric titration curves of compound **1** ($C_L = 6.7 \times 10^{-4}$ M) in 50% w/w DMSO/water; b) Absorption spectra of **1** (2.56 < pH < 11.53, $C_L = 4 \times 10^{-5}$ M) in 50% w/w DMSO/water and outset containing the individual calculated spectra by PSEQUAD [10].

Table 1 – Stepwise protonation constants of compound **1** and compound 2 for comparison purpose, as well as global formation constants[a] for their Cu(II) and Zn(II)) complexes (T = 25.0 ± 0.1 °C, I = 0.1 M KCl, 50% w/w DMSO/water) and pM[b] values.

Compound	$M_mH_hL_l$	log K_i	log $\beta_{Cu_mH_hL_l}$	log $\beta_{Zn_mH_hL_l}$
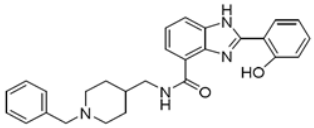 **1**	(011)	8.98(2)[c] 9.00(1)[d]		
	(021)	7.78(4)[c] 7.11(3)[d]		
	(031)	2.86(5)[c] 2.38(8)[d]		
	(111)		18.96(8)[c] 18.864(6)[d]	13.81(7)[c]
	(101)		11.71(7)[c] 13.08(2)[d]	-
	(1-11)		4.44(4)[c] 5.12(2)[d]	
	(122)		37.27(5)[c] -	26.51(9)[c]
	(102)		22.18(9)[c] 19.18(9)[d]	-
	(1-12)		14.64(6)[c] -	3.77(8)[c]
	pM		14.3[c] 13.9[d]	6.4[c]
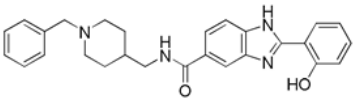 **2** [e]	(011)	8.671(1)		
	(021)	7.39(1)		
	(031)	3.21(1)		
	(111)		16.43(4)	13.13(3)
	(122)		32.13(4)	25.24(8)
	(102)		17.91(4)	9.94(8)
	(1-12)		8.20(6)	-
	pM		10.7	6.3

[a] $\beta_{M_mH_hL_l} = [M_mH_hL_l]/[M]^m[H]^h[L]^l$; [b] pM = −log[M] at pH 7.4 (C_L/C_M = 10, C_M = 10^{-6} M), [c] pH-potentiometric data; [d] UV-vis spectrophotometric data; [e] ref. [18].

Compound **1** was isolated in its neutral mono-protonated form (HL, a = 0 in **Fig. 1a)**) after the synthetic procedure, although the fully protonated species corresponds to H_3L^{2+}. The three protonation constants contained in **Table 1** for compound **1** are in accordance, as expected, to those previously obtained for compound **2** and correspond to the protonation of the phenolic oxygen of the BIM moiety (log K_1), then the N-piperidine nitrogen atom (log K_2) and finally the imidazole nitrogen N(3) of the BIM portion (log

K_3) [18]. The values obtained by both experimental techniques (potentiometry and UV-vis spectrophotometry) are quite similar for log K_1 values but present some discrepancies for log K_i (i =2,3), probably due to the fact that the UV-vis spectrophotometric titrations have higher experimental errors also since they are not performed in automated manner as the potentiometric ones.

Taking into consideration the outset in **Fig. 1b)**, enclosing the calculated spectra by PSEQUAD of the different protonated species for compound **1,** it is possible to see that: the fully protonated species (H_3L^{2+}) has three absorption maxima at 306, 334 and 343 nm; the absorption at 332 nm correspond to both di- and mono-protonated species (H_2L^+ and HL); the mono-protonated HL and the deprotonated L^- species have a large absorption band with maximum at ca 373 nm. Moreover, at pH 7.4 and considering $C_L = 10^{-5}$ M, as an attempt to mimic the physiological conditions, the predominant species is: for compound **1**, H_2L^+ (70%) with a contribution of 29% of the neutral HL species; for compound **2**, the neutral HL (50%) and 48% of H_2L^+. Even though the lipo-hydrophilic character is not only determined by the molecular charge but also by the ability to establish solute-solvent interactions, the existence of the neutral HL species in significant concentrations (ca 29-50%) explains the need of using a 50% w/w DMSO/water medium in the solution studies. In fact, in particular compound **2** showed to be insoluble for inferior % of DMSO content in the DMSO/water mixtures.

3.4. *Metal chelation*

3.4.1. *Solution equilibrium studies*

The existence of a BIM moiety in the structure of potential anti-neurodegenerative drugs was already proven to endow the compounds with capacity for hitting several AD targets, such as biometal chelation, eventual dual AChE interaction, as well as self- and Cu-mediated Aβ aggregation [18-20]. Concerning metal chelation, the BIM unity is a bidentate moiety and its (*N*,*O*) coordination mode implicates a good potential coordination towards *hard-soft* metal ions. The study of the metal chelating properties of compound **1**, a positional isomer of the already studied compound **2**, containing the BIM unit *ortho*-attached to the benzylpiperazinic moiety, will also show the possibility of formation of a (*N*,*O*,*O*) metal coordination type involving both the BIM moiety and the adjacent carbonyl oxygen atom.

The chelating ability of compound **1** was studied by using the same experimental techniques (potentiometry, UV-vis spectrophotometry) and experimental medium used

for the titration of the ligand alone (50% w/w DMSO/water). In the following calculations for the 1:1 and 1:2 M/L systems (M = Cu, Zn), the log K_i values previously obtained by each experimental method will be used in the complexation studies performed by the same methodology. **Fig. 1a)** evidences an alteration in the deprotonation profile of the ligand titration curve due to the presence of the metal ion since the curves for the M(II)/L systems lye well below that of the ligand for $a > -2$ (M = Cu) or $a > -1$ (M = Zn), thus supporting the formation of metal complexes with the deprotonated (L^-) and mono-protonated (HL) forms of the ligand with comparative stability order Cu > Zn. The potentiometric curves seem to be in accordance with a (*N*,*O*) coordination mode, involving the BIM moiety of compound **1**, as already found for other BIM derivatives [18,21]. **Table 1** contains the equilibrium models obtained from the fitting analysis of the potentiometric curves (M = Cu, Zn) and the UV-vis spectral data (M = Cu).

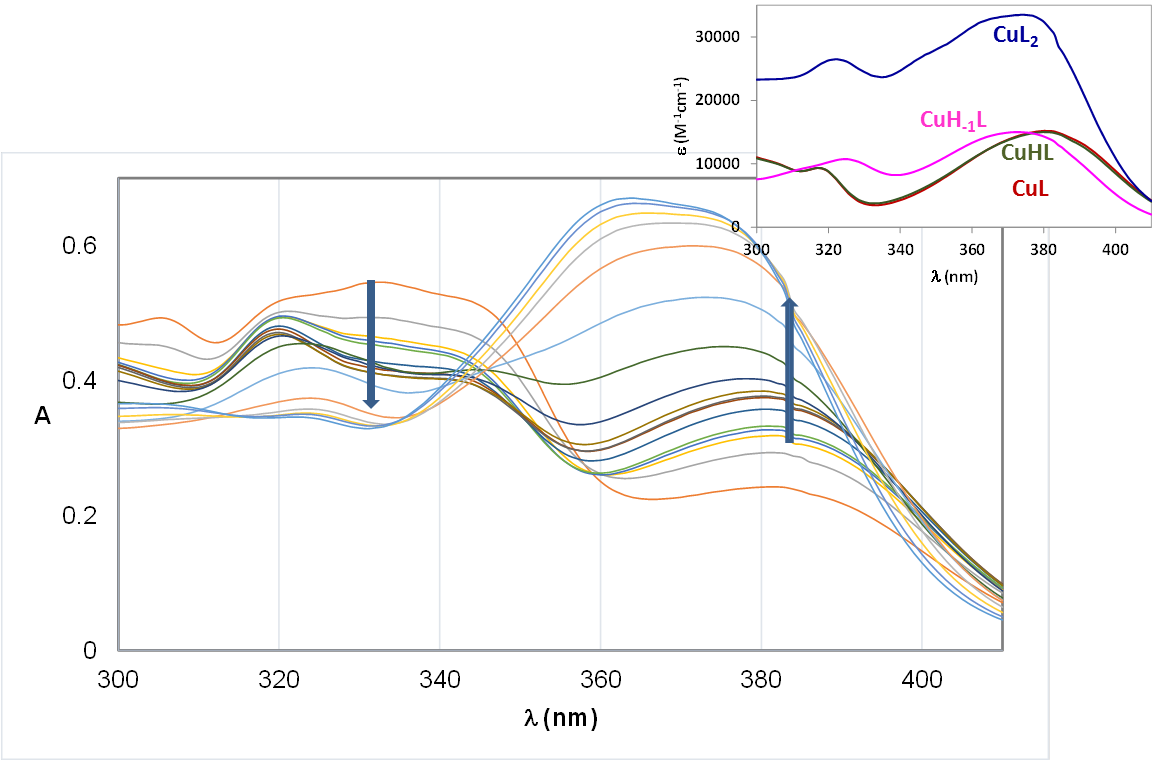

Figure 2 - Spectrophotometric absorption spectra of the 1:2 Cu^{2+}/ **1** system (2.58 < pH < 11.51, $C_L = 4.0 \times 10^{-5}$ M) in 50% w/w DMSO/water and outset and outset containing the individual calculated spectra by PSEQUAD [10].

In the obtained metal complex models, MHL and MH_2L_2 (not found from 1:2 Cu^{2+}/**1** spectral data) correspond to species with the ligand containing one protonated nitrogen

atom at the piperidine moiety, while ML and ML_2 correspond to complexes involving the completely deprotonated form of the ligand; $MH_{-1}L$ and $MH_{-1}L_2$ (not found from 1:2 Cu^{2+}/**1** spectral data) are mixed ligand-hydroxo metal complexes. The models obtained for Cu^{2+}/**1** system from potentiometric and spectrophotometric data (see **Table 1**) are not identical but quite similar.

The outset of **Figure 2** evidences that the calculated spectra (λ_{max} (ε, $M^{-1}cm^{-1}$) at 317 nm (9.3×10^3) and 380 nm (1.5×10^4)) for both CuHL and CuL complexes are equal, resulting from the fact that the coordination core is exactly the same and so the piperidinic nitrogen does not contribute to the copper coordination as already found for compound **2** [18]; the intensity of the calculated spectrum rises for the CuL_2 species, that displays λ_{max} (ε, $M^{-1}cm^{-1}$) values corresponding to a shoulder at 361 nm (3.2×10^4) and a band at 374 (3.4×10^4) nm. As expected, to the $CuH_{-1}L$ species corresponds also a more intense spectrum with a blue shift of the bands relatively to CuHL/CuL (372 nm (1.5×10^4)), corresponding to the formation of a complex that has an additional coordination site occupied by an apical water molecule.

Comparing, the spectral data of the Cu^{2+}/ **1** and Cu^{2+}/**2** systems [18], the most striking difference relates to the spectra of the CuHL species, with λ_{max} at 320, 335 and 365 nm. The inexistence, in this last case, of a band at 380 nm may point towards the formation of a MHL complex with a coordination core more strained in the case of compound **1** than for compound **2**.

Figure 3 shows the species distribution curves for the 1:2 Cu(II)/**1** and Zn(II)/**1** systems by using the potentiometric determined model at the used experimental conditions.

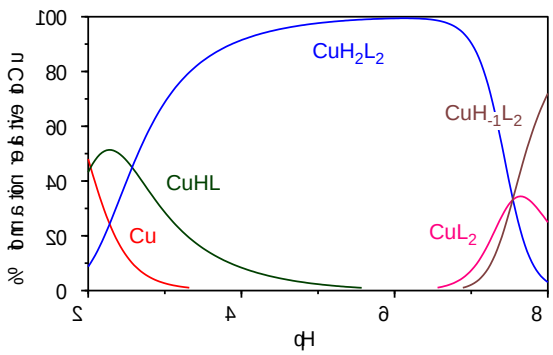

a)

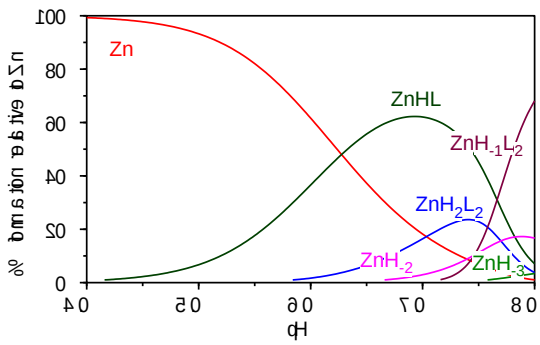

b)

Figure 3 - Species distribution curves for the 1:2 M/**1** systems: a) M = Cu; b) M = Zn (C_L = 6.7 ×10^{-4} M).

Comparison of the metal chelating capacity of compound **1** with that of the already studied analogous compound **2** (see **Table1**) reveals that the pM values (at pH 7.4, C_L/C_M = 10, $C_M = 10^{-6}$ M) are analogous for zinc but higher for copper, which may point towards the possibility of compound **1** having a different copper coordination core, eventually including the adjacent carbonyl oxygen atom, with correspondingly higher stability of the copper complex with **1**. In fact, previous studies on the copper chelation ability of 8-hydroxyquinoline (HQ, pCu=13.2 in 60% w/w DMSO/water) [22], a commonly known stong chelator, reveals that compound **1** presents a slightly higher Cu^{2+} chelating capacity than HQ while compound **2** shows a small reduction.

To further examine the proposed complexation models, ESI-MS data was also obtained from solutions of M/**1** (M = Cu, Zn), in 50% w/w DMSO/H_2O and 1:1 and 1:2 M/L stoichiometric conditions, at specific pH values. The obtained spectra confirmed the existence of 1:1 and 1:2 metal complexes (see **Table 2** and **Figure 4**). The ESI-MS analysis of a solution of the 1:1 Cu^{2+}/**1** system, at pH 4.28 and in the negative mode, showed a group of peaks at m/z 571/573, suggesting a characteristic isotopic distribution of a $[Cu(L\text{-}H)Cl_2]^-$ species. However, due to the lower intensity of the signal, a clear fit with a calculated isotopic distribution for $[(C_{27}H_{27}N_4O_2)CuCl_2]^-$ was not achieved.

Table 2 – ESI-MS ions for the Cu^{2+} and Zn^{2+} complexes of compound **1** in 50% w/w DMSO/H_2O (1:2 M/L, C_L = 2.25 × 10^{-4} M).

Species	pH	M = Cu (m/z)	M = Zn (m/z)
$[M(L\text{-}H)Cl_2]^-$	7.01	-	573.2/575.2/577.1
$[M(L\text{-}H)L]^+$	6.42	942.2/944.2	-
$[M(L\text{-}H)L]^+$	8.39	-	943.2/945.2

L represents the neutral mono-protonated form of compound **1**

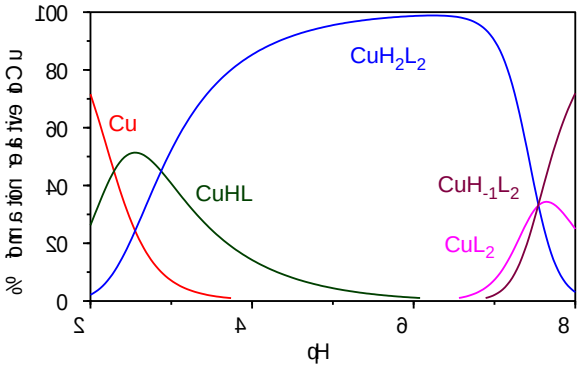

Cu
CuHL
CuH2L2
CuH-1L2
CuL2

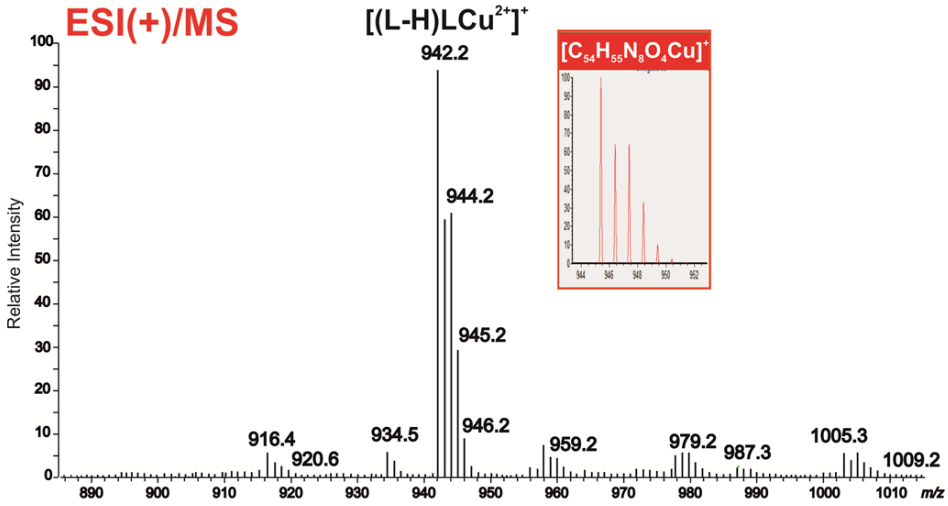

ESI(+)/MS
[(L-H)LCu2+]+
[C54H55N8O4Cu]+
Relative Intensity
942.2
944.2
945.2
946.2
916.4
920.6
934.5
959.2
979.2
987.3
1005.3
1009.2
m/z

a)

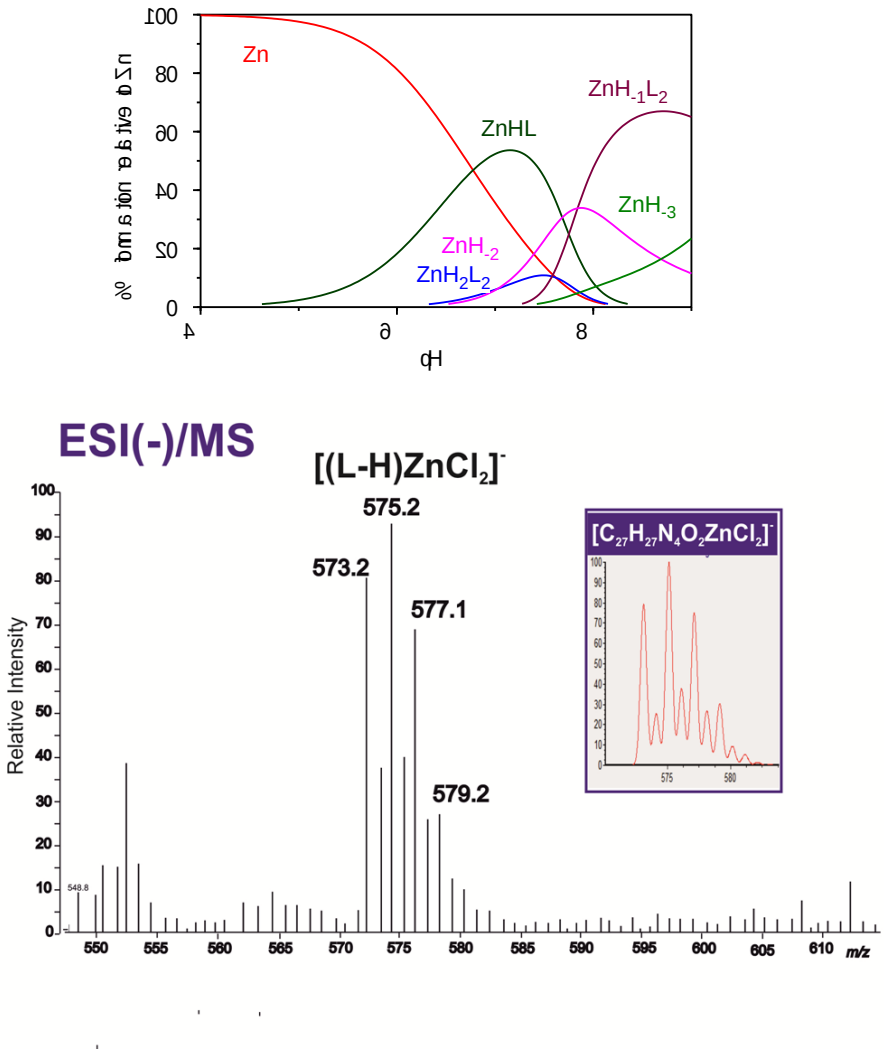

b)

Figure 4 - a) Expanded ESI(+) mass spectrum for the Cu(II)/**1** system (C_L/C_{Cu} = 2, C_L = 2.25 × 10^{-4} M, pH=6.42) and species distribution curves. The insert shows the theoretical isotopic pattern for $[(C_{54}H_{55}N_8O_4)Cu]^+$; b) Expanded ESI(-) mass spectrum for the Zn(II)/**1** system (C_L/C_{Zn} = 2, C_L = 2.25 × 10^{-4} M, pH=7.01) and species distribution curves. The insert shows the theoretical isotopic pattern for $[(C_{27}H_{27}N_4O_2)ZnCl_2]^-$.

Finally, to analyze the copper coordination core of the complexes with compounds **1** and **2**, EPR spectra of these copper systems were obtained, at room temperature and in frozen solution together with the calculated EPR spectra of the component species (see **Figure 5**). The solution EPR spectra for the studied systems could be mainly described by free copper, CuLH and CuL_2H_2, as well as the ratio of the species agreed well with the distribution curves at the selected pH working values. For the systems with compound **1**

(1:1) in RT solution and **2** in frozen solution, only the CuLH complex or the free copper and CuLH could be detected, respectively. In those cases, the 1:2 Cu/L complex was not formed. Nevertheless, for compound **1,** the frozen solution sample recorded at 1:1 ratio showed a dimer species ($Cu_2L_2H_2$), besides CuLH, which frequently forms for aromatic flat ligands by the off-centered parallel stacking interaction of two mono-complexes arranged above each other. The frozen solution spectra of the CuLH and CuL_2H_2 complexes show well resolved nitrogen splitting, and could be simulated with one nitrogen for CuLH and two nitrogens for CuL_2H_2, in accordance with the involvement of one or to BIM chelating cores. The obtained EPR data are collected in **Table 3**.

The comparison of the EPR data for the CuLH complexes of compounds **1** and **2** allows concluding that the isotropic and anisotropic g values reflect higher ligand field for compound **1** than for compound **2**, since the g values are lower for compound **1**. This result supports the already suggested (*N*,*O*,*O*) tridentate coordination mode for compound **1**, with the involvement of the adjacent carbonyl oxygen atom. For the 1:2 copper complex of compound **1** it is probable that the second ligand coordinates equatorially with its imidazole nitrogen and axially with the phenolate oxygen atom. This coordination change agrees with the facts that g_z value decreases only 0.01, comparing with the same value of the 1:1 complex, and the A_z value also declines evidencing an axial coordination with small rhombic distortion.

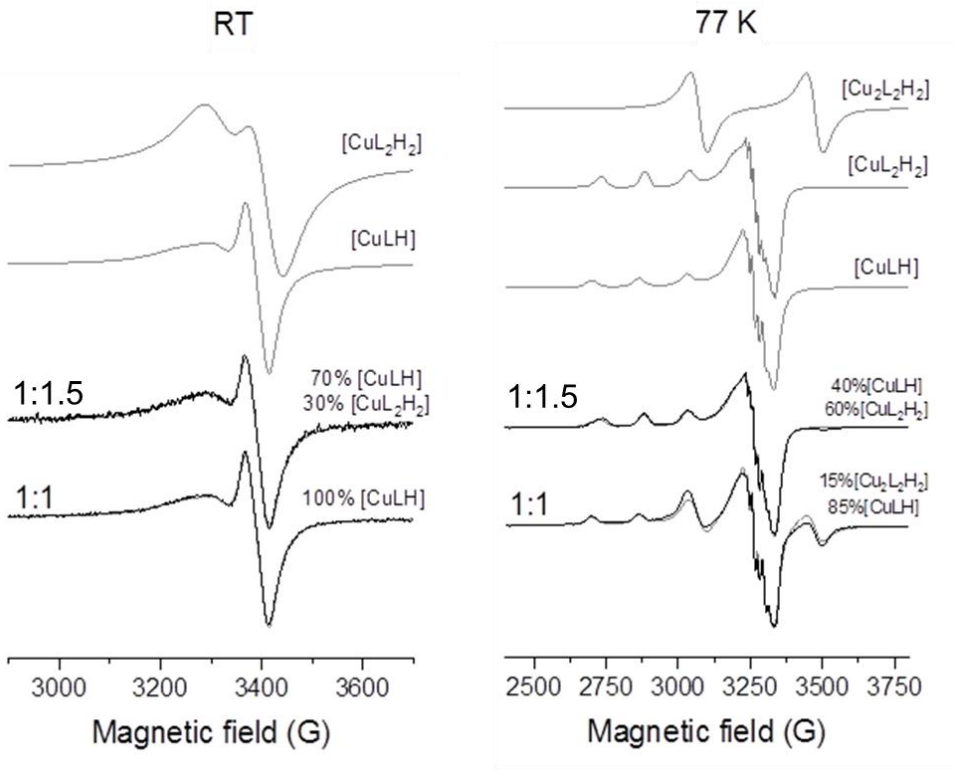

a)

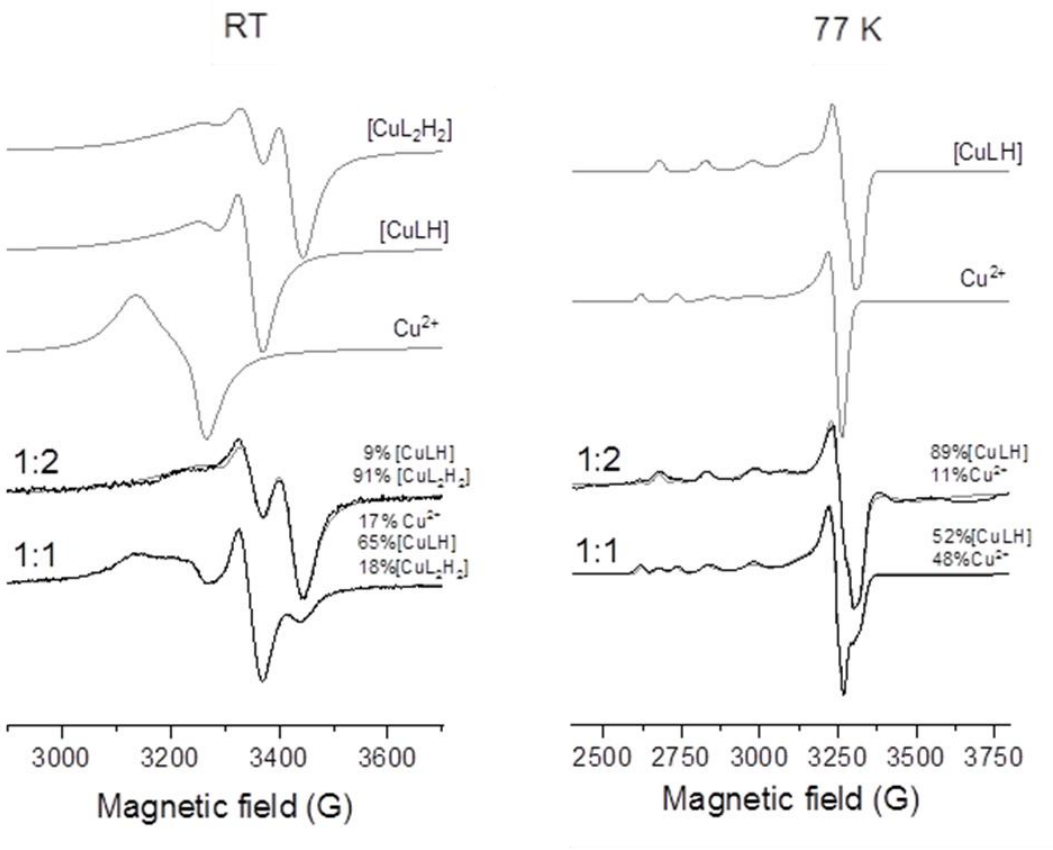

b)

Figure 5 - Measured (black) and calculated (grey) EPR spectra obtained for a) Cu^{2+}/**1** 1:1 (pH = 6.75) and 1:1.5 (pH = 6.91); b) Cu^{2+}/**2** 1:1 (pH = 5.46) and 1:2 (pH = 5.72) systems at room temperature (left) and in frozen solution (right).

Table 3 - Isotropic and anisotropic EPR parameters obtained for the Cu^{2+} complexes with compounds **1** and **2**[a]

Compound/species	g_0	A_0/G	a_0^N/G	$g_{0,calc}$[b]	g_x	g_y	g_z	A_x/G	A_y/G	A_z/G	a_x^N/G	a_y^N/G	a_z^N/G
1													
CuLH	2.123	54.9	14.5	2.134	2.058	2.057	2.287	15.8	16.2	161.4	14.2	17.3	4.8
CuL_2H_2	2.120	66.0	14.5	2.127	2.048	2.059	2.275	20.7	3.9	149.0	14.5	15.0	9.9
											10.1	11.9	10.3
$Cu_2L_2H_2$[c]	2.066												
2													
Cu	2.194	31.6		2.196	2.086		2.417	6.9	110				
CuLH	2.156	59.6	13.6	2.148	2.060		2.324	15.2		145	14.1	14.1	10.0
CuL_2H_2	2.111	61.3	10.8										

[a] The experimental errors were ± 0.002 for g_x and g_y and ± 0.001 for g_z and g_0; ±2 G for A_x and A_y and ± 1 G for A_z and A_0.
[b] Calculated by the equation $g_{0,calc} = (g_x + g_y + g_z) / 3$.
[c] The dimer species was calculated as a doublet. The peak distances resulted in the dipolar coupling of D = 287 G, from which the copper-copper distance of 4.14 Å can be calculated.

So, the spectral data collected, namely EPR information, and the callculated equilibrium models obtained for compound **1** point towards a chelating core composed by the N(3)

imidazole and O-phenol atoms of the ligands, excluding the hypothesis of metal coordination through the distant nitrogen atom of the piperidine [18], but eventually including the adjacent carbonyl oxygen atom in the case of the copper complexes.

3.4.2. *Molecular modeling of the copper complexes*

In the absence of X-ray structures, a molecular modelling study was accomplished aimed at providing some further insight into the 1:1 copper complex structures with compounds **1** and **2**. In that way, a tridentate (*N*,*O*,*O*) coordination mode was considered for compound **1**, involving one coordinated water molecule, while a bidentate (*N*,*O*) coordination type was adopted for compound **2** and two coordinated water molecules were included in the chelating core. These studies were carried out with full geometry optimization of the Cu^{2+} complexes by quantum mechanical calculations based on DFT methods [23] included in the Gaussian 03 program software [12] with the B3PW91 functional [24]. Geometry optimizations were obtained by using 3-21G basis set [25] for all elements, first, and afterwards re-optimized using 6-31G** [26] for the main group elements and the Stuttgart–Dresden pseudopotential and associated basis set for Cu (SDD [27]). No symmetry constrains were enforced during geometry optimizations. The calculations were performed as well for one water molecule by using the B3PW91 functional, first with the 3-21G basis set and subsequently re-optimized via 6-31G** basis set.

The energy-minimized structures of the copper complexes present a distorted tetrahedral square planar four-coordinate configuration for **1** while for **2** corresponds a distorted tetrahedral geometry (see **Figure 6**).

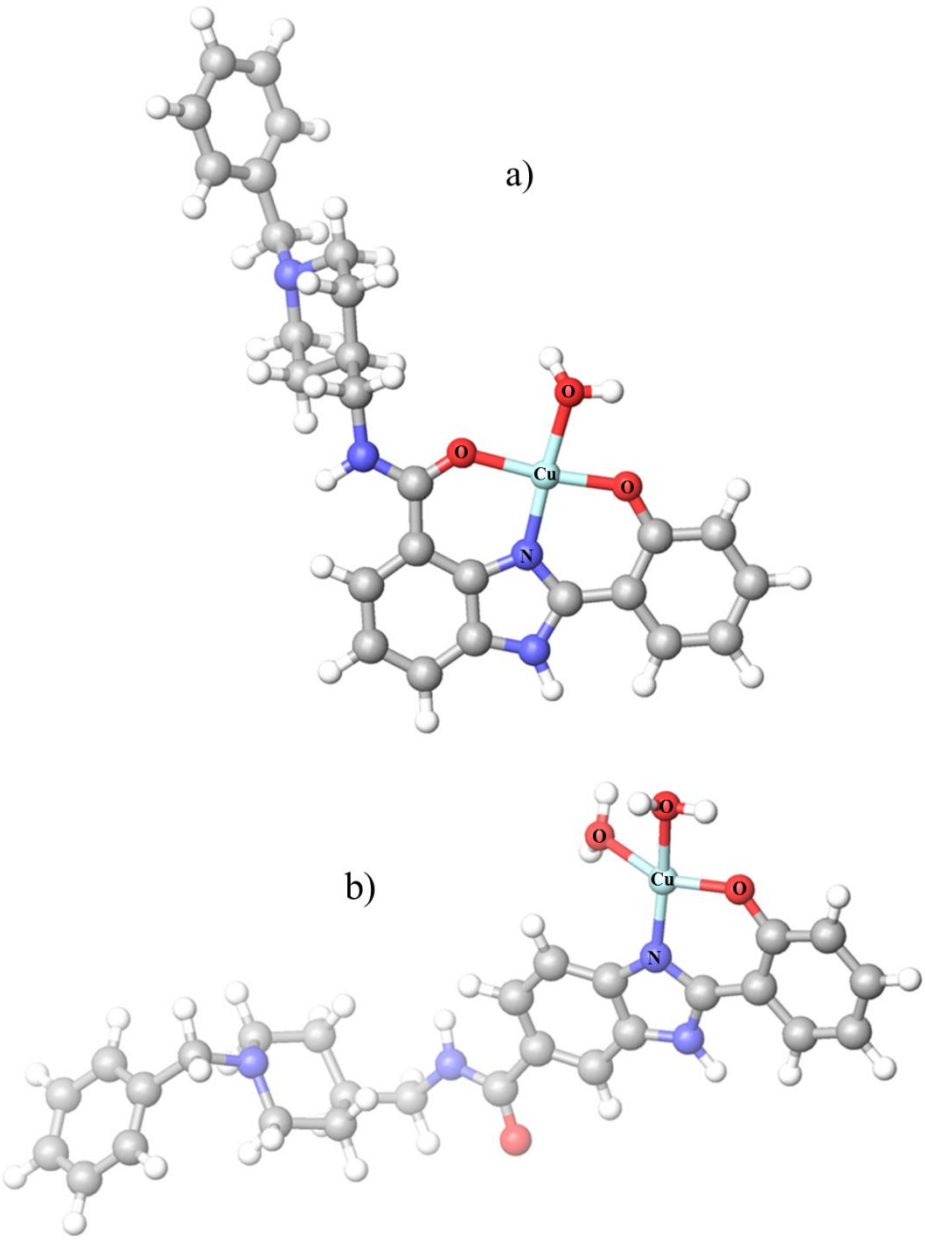

Figure 6 – DFT-minimized structures of 1:1 copper complexes with compound a) **1** and b) **2**. Coloring of atoms: Cu light blue, N blue, O red, C grey and H white.

In the obtained modeling simulations, some identical coordination bond distances can be found between the two structures for Cu-H_2O (2.02-2.05 Å) and Cu-*O*-phenol (1.86-1.88 Å), while the Cu-N distance increases somehow from the copper complex with **1** (1.88 Å) to that with **2** (1.91 Å), probably due to the stronger tridentate coordination established in the case of complex with **1**, that also involves the adjacent *O*-carbonyl atom (distance Cu-*O*-carbonyl 1.96 Å). In the case of the complex with compound **1**, the distortion in relation to a regular square planar geometry is well demonstrated by the coordination

bond angles (83.6-93.0^0) and the almost planar geometry as showed by the bond angles of *O*-phenol-Cu-*O*-carbonyl (173.1^0) and N-Cu-water (174.8^0). On the other hand, the copper coordination with compound **2** also exhibits a strong distortion from a tetrahedral geometry, with coordination bond angles ranging from 82.4 to 99.7^0.

Since these two complexes do not have exactly the same number of atoms, comparison of complex stability was based on the determination of the free energy difference (ΔG = 25.6 Kcal/mol) between Cu-**1** complex plus one water molecule and Cu-**2** molecule. Therefore, the calculations show that the copper complex with compound **1** is more stable than that with compound **2**, which is according to the previously presented solution studies.

3.5. *Biological activity*

3.5.1. AChE and Aβ aggregation inhbitory activity

Compound **1** under study was assayed for AChE inhibition through a reported method [29] and proved to have a quite good activity (IC_{50} = 9 μM), analogous to that of compound **2** (see **Table 4**), which is supported by the docking simulations. Actually, previous studies already revealed that compounds with BIM motif have good AChE inhibitory capacity, in low micromolar range [18-20], although presenting higher values than the parent compound DNP. Even so, this last fact does not abolish the purpose of the suggested drug design since in multifactorial diseases the advantages of using a multi-target drug can overcome the disadvantage of losing some specific property corresponding to a unique target drug.

Table 4 – Biological properties of compounds **1** and **2**: inhibition of AChE (Electric eel), self-mediated and Cu-induced Aβ_{1-42} aggregation as well as some predicted pharmacokinetic parameters.

Compound	EeAChE (IC_{50}, μM)[a]	Aβ aggreg (%)[b] self-med	Aβ aggreg (%)[b] Cu-ind	log $P^{c,d}$	log $BB^{c,e}$
1	9 ± 1	38.6	58.9	4.35	-0.64
2	4.2 ± 0.8[f]	48.8	69.0	4.39	-0.73
DNP[f]	0.026	-	-	4.43	0.13

[a] mean ± SEM (standard error of the mean) of 3 experiments for 50% inhibition of electric eel AChE (EeAChE); [b] Inhibiton of self- and Cu-mediated Aβ_{1-42} aggregation by thioflavin-T fluorescence method; measurements in presence of inhibitor (40 μM)

for 40 μM Aβ_{1-42} and the values are mean of three independent measurements in duplicate (SEM < 10%); [c] predicted values using QikProp program, v. 2.5, ref. [7]; [d] octanol/water partition coefficient; [e] brain/blood partition coefficient; [f] ref. [28]

The anti-amyloidogenic capacity of compound **1**, in the absence and in the presence of copper, was evaluated based on the measurement of the fluorescence emission of Thioflavin T (ThT) associated to fibril binding [15,16]. Due to solubility problems of compound **1** in the phosphate buffer (0.215 M, pH 8.0) working medium, the assays were accomplished in the presence of 40 μM concentration of inhibitor, instead of 80 μM [18,20], and so the same procedure was adopted for compound **2** for comparison reasons (see **Table 4**). The obtained data show that both compounds induce a decrease on the ThT fluorescence associated with Aβ fibril binding. In fact, they inhibit the Aβ_{1-42} self-aggregation process with good capacity, slightly higher for the positional isomer **2** than for compound **1**, probably due to conformational reasons in the ligand intercalation between the Aβ fibrils. In terms of the inhibition of Cu-induced Aβ aggregation, the compounds induce an analogous increase (20.2-20.3%) when comparing with their corresponding capacity for self-inhibition, in accordance with their good chelating capacity towards copper. Nevertheless, these chelators have conditional dissociation constants (K'_d) for the copper complexes at pH 7.4 of 254 picomolar (**1**) and 34 nanomolar (**2**), these values being outside the proposed range K'_d = 1-10 picomolar corresponding to chelators eventually able to retrieve copper from Aβ peptide (K'_d = 10 picomolar – 100 nanomolar for Cu(Aβ) complexes) [30]. In this way, there is no competition for copper between these BIM hybrids and Aβ peptide, the inhibition process being apparently mainly due to ligand intercalation between the β-sheets of Aβ fibrils.

In order to assess the potential of compound **1** as an eventual drug, some indicators of its pharmacokinetic profiles were calculated with QikProp program [7]. Parameters such as the lipo-hydrophilic character (log *P*), the ability to cross the blood-brain barrier (log *BB*), the ability to be absorbed through the intestinal tract to the blood (Caco-2 cell permeability), and the verification of *Lipinski's rule of five*, can give an idea of its druglikeness for oral administration as an anti-AD drug. Both the positional isomers have the same molecular weight (440.5) lower than 500 and present similar lipo-hydrophilic character and no violations of the Lipinski´s rule,`s, although the slightly higher values for log *P*, log BB and caco permeability can be responsible for the slightly better CNS activity predicted for the isomer **1** as compared with **2**. In summary, both positional

isomers present good BBB permeability (log BB) and can be eligible as drug candidates for oral administration.

Table 5 - Pharmacokinetic properties as predicted *in silico* by software QikProp v.2.5[7].

Comp.	MW (Da)	clog *P*	log BB	Caco-permeability (nm/s)	CNS	Violations of Lipinski's rule
1	440.54	4.352	-0.638	225	+/-	0
2	440.54	4.386	-0.730	194	-	0

3.5.2. Cell viability and neuroprotection

Using neuroblastoma SHSY-5Y cells the potential therapeutic effect of compound 1 was tested exposing these cells to Aβ1–42 peptides. For this new compound 1 a dose–response curve was performed to select a nontoxic concentration in order to analyze the neuroprotective effect (Fig. S2). It was observed that Aβ1–42 induced a decrease in cell viability and, interestingly, compound 1 completely prevented Aβ1–42 cellular toxicity, as cells present relative viability values comparable to untreated cells (see Fig. 10). In opposition, cells treated with Fe/Ascorbate have a decrease in cell viability which compound 1 could not prevent. These results demonstrate that the ortho-positional isomer (1) has a higher neuroprotective role than the positional isomer 2 [17], and thus a higher specificity against Aβ-induced cell toxicity.

4. Conclusions

A new DNP-BIM hybrid (compound 1), with the BIM unit orthoattached to the benzylpiperazinic moiety, was synthesized and studied with the aim of evaluating the effect of the imposed structural modification over its physico-chemical and biological properties as potential anti-AD drug, in comparison with a previously developed positional isomer (compound 2). Compound 1 was found to have a higher chelating capacity towards Cu2+ (pCu = 14.3, pZn = 6.4, pH 7.4, CL/ CM = 10, CM = 10−6 M) than compound 2 (pCu = 10.7, pZn = 6.3), due to the 1-order increasing of denticity, that allows the formation of a (N,O,O) coordination core for Cu2+, as proved by EPR and molecular modeling data of the copper complexes. Concerning the biological properties, both compounds present good AChE inhibition (low micromolar range), in accordance with the docking studies, and are moderate/good inhibitors of Aβ self- and Cu-mediated aggregation. Since there is no competition for copper between these BIM hybrids and Aβ

peptide, the inhibition process appears to be mainly due to ligand intercalation between the β-sheets of Aβ fibrils. Therefore, the herein compiled data allows concluding that afterapplying a structural change over the already studied compound 2, for the sake of increasing ligand denticity and thus improving the metal chelating capacity as well as the control/modulation of interconnected multiple pathological aspects of AD, the obtained compound 1 presents quite analogous AChE and Aβ self- and Cu-mediated aggregation inhibitory capacity, being also eligible as drug candidate for oral administration and with improved neuroprotective role against Aβ-induced cell toxicity.

Abbreviations

Acetylcholinesterase	AChE
Acetylcholinesterase inhibitor	AChEI
Acetylthiocholine iodide	AChI
Alzheimer's disease	AD
Blood-brain	BB
Hydroxyphenyl-benzimidazole	BIM
β-amyloid	A β
Cationic active site	CAS
Central nervous system	CNS
Charge transfer	CT
Donepezil	DNP
Donepezil based hydroxyphenyl-benzimidazole	DNP-BIM
Bis(3-carboxy-4-nitrophenyl) disulfide	DTNB
Electron paramagnetic resonance spectroscopy	EPR
Electrospray mass spectroscopy	ESI-MS
4-(2-Hydroxyethyl)-1-piperazineethanesulfonic acid	HEPES
1,1,1,3,3,3–Hexafluoro-2-propanol	HFIP

3-(4,5-dimethylthiazol-2-yl)-2,5-diphenyltetrazolium bromide	MTT
Nuclear magnetic resonance spectroscopy	NMR
Peripheral anionic site	PAS
Thioflavin T	ThT
Tris(hydroxymethyl)aminomethane	TRIS
Ultraviolet-visible spectrophotometry	UV-vis

Acknowledgements

The authors acknowledge the Portuguese *Fundação para a Ciência e Tecnologia* (FCT) for the projects UID/QUI/00100/2013, UID/QUI/00100/2019, and also the Portuguese NMR (IST-UL Center) and Mass Spectrometry Networks (Node IST-CTN) for providing access to their facilities, as well as to Dr. Conceição Oliveira for the collaboration in the mass spectra interpretation. The EPR studies were supported by the J. Bolyai Research Scholarship (N.V.M., BO/00109/17/7) of the Hungarian Academy of Sciences. We also thank the Erasmus fellowship (R.J.) from Europe Erasmus+ program.

References

[1] Alzheimer''s Association, Alzheimer's disease facts and figures, Alzheimers Dement. 15 (2019) (2019) 321–387.

[2] a) J.L. Cummings, T. Morstorf, K. Zhong, Alzheimers Res. Ther. 6 (2014) 37;

b) J. Marco-Contelles, ACS Chem. Neurosci. 10 (2019) 1127–1128.

[3] A. Rinaldi, EMBO Rep. 19 (2018) e46714.

[4] A.C. Tricco, H.M. Ashoor, C. Soobiah, et al., J. Am. Geriatr. Soc. 66 (2018) 170–178.

[5] R. Jakob-Roetne, H. Jacobsen, Angew. Chem. Int. Ed. 48 (2009) 3030–3059.

[6] S.A. James, I. Volitakis, P.A. Adlard, J.A. Duce, C.L. Masters, R.A. Cherny, A.I. Bush, Free Radic. Biol. Med. 52 (2012) 298–302.

[7] M.G. Savelieff, S. Lee, Y. Liu, M.H. Lim, ACS Chem. Biol. 8 (2013) 856–865.

[8] K.P. Kepp, R. Squitti, Coord. Chem. Rev. 397 (2019) 168–187.

[9] a) A.L. Hopkins, Nat. Chem. Biol. 4 (2008) 682–690;

b) A. Cavalli, M.L. Bolognesi, A. Minarini, M. Rosini, V. Tumiatti, M. Recanatini, C. Melchiorre, J. Med. Chem. 51 (2008) 347–372.

[10] M.J. Oset-Gasque, J. Marco-Contelles, ACS Chem. Neurosci. 9 (2018) 401–403.

[11] R.R. Ramsay, M.R. Popovic-Nikolic, K. Nikolic, E. Uliassi, M.L. Bolognesi, Clin. Transl. Med. 7 (2018) 1–14.
[12] M.A. Santos, K. Chand, S. Chaves, Fut. Med. Chem. 8 (2016) 2113–2142.
[13] M.A. Santos, K. Chand, S. Chaves, Coord. Chem. Rev. 327–328 (2016) 287–303.
[14] K. Chalupova, J. Korabeccny, M. Bartolini, B. Monti, D. Lamba, R. Caliandro, A. Pesares, X. Brazzolotto, A.-J. Gastellier, F. Nachon, J. Pejchal, M. Jarosova, D. Jun, M. Hrabinova, R. Dolezal, J. Karasova, M. Mzik, Z. Kristofikova, J. Misik, L. Muckova, P. Jost, O. Soukup, M. Benkova, V. Setnicka, L. Habartova, M. Chvojkova, L. Kleteckova, K. Vales, E. Mezeiova, E. Uliassi, M. Valis, E. Nepovimova, M.L. Bolognesi, K. Kuca, Eur. J. Med. Chem. 168 (2019) 491–514.
[15] K. Spilovska, J. Korabecny, E. Nepovimova, R. Dolezal, E. Mezeiova, O. Soukup, K. Kuca, Curr. Top. Med. Chem. 17 (2017) 1006–1026.
[16] A. Hiremathad, R.S. Keri, A.R. Esteves, S.M. Cardoso, S. Chaves, M.A. Santos, Eur. J.
Med. Chem. 148 (2018) 255–267.
[17] L. Piemontese, D. Tomás, A. Hiremathad, V. Capriati, E. Candeias, S.M. Cardoso, S. Chaves, M.A. Santos, J. Enzyme Inhib, Med. Chem. 33 (2018) 1212–1224.
[18] W.L.F. Armarego, D.D. Perrin, Purification of Laboratory Chemicals, fourth ed., Butterworth-Heinemann, Oxford, 1999.
[19] G. Kryger, I. Silman, J.L. Sussman, Structure Fold. Des. 7 (1999) 297–307 http://www.rcsb.org/pdb/explore/explore.do?structureId=1EVE.
[20] Maestro, version 9.3, Schrödinger Inc., Portland, OR, 2012.
[21] T. Hassinen, M.J. Peräkylä, J. Comput. Chem. 22 (2001) 1229–1242.
[22] M. Clark, R.D. Cramer III, N.J. Van Opdenbosch, J. Comput. Chem. 10 (1989) 982–−1012.
[23] G. Jones, P. Willett, R.C. Glen, A.R. Leach, R. Taylor, J. Mol. Biol. 267 (1997) 727–748.
[24] QikProp, version 2.5, Schrödinger, LLC, New York, NY, 2005.
[25] F.J.C. Rossotti, H. Rossotti, J. Chem. Ed. 42 (1965) 375–378.
[26] A. Gans, A. Sabatini, A. Vacca, Talanta 43 (1996) 1739–1753.
[27] L. Zékány, I. Nagypál, G. Peintler, PSEQUAD version 5 (2001) 01.
[28] K.N. Raymond, C.J. Carrano, Acc. Chem. Res. 12 (1979) 183–190.
[29] A. Rockenbauer, L. Korecz, Appl. Magn. Reson. 10 (1996) 29–43.
[30] R.G. Parr, W. Yang, Density Functional Theory of Atoms and Molecules, Oxford

University Press, New York, 1989.
[31] M.J. Frisch, G.W. Trucks, H.B. Schlegel, G.E. Scuseria, M.A. Robb, J.R. Cheeseman,
J.A. Montgomery Jr., T. Vreven, K.N. Kudin, J.C. Burant, J.M. Millam, S.S. Iyengar,
J. Tomasi, V. Barone, B. Mennucci, M. Cossi, G. Scalmani, N. Rega, G.A. Petersson,
H. Nakatsuji, M. Hada, M. Ehara, K. Toyota, R. Fukuda, J. Hasegawa, M. Ishida,
T. Nakajima, Y. Honda, O. Kitao, H. Nakai, M. Klene, X. Li, J.E. Knox,
H.P. Hratchian, J.B. Cross, V. Bakken, C. Adamo, J. Jaramillo, R. Gomperts,
R.E. Stratmann, O. Yazyev, A.J. Austin, R. Cammi, C. Pomelli, J.W. Ochterski,
P.Y. Ayala, K. Morokuma, G.A. Voth, P. Salvador, J.J. Dannenberg,
V.G. Zakrzewski, S. Dapprich, A.D. Daniels, M.C. Strain, O. Farkas, D.K. Malick,
A.D. Rabuck, K. Raghavachari, J.B. Foresman, J.V. Ortiz, Q. Cui, A.G. Baboul,
S. Clifford, J. Cioslowski, B.B. Stefanov, G. Liu, A. Liashenko, P. Piskorz,
I. Komaromi, R.L. Martin, D.J. Fox, T. Keith, M.A. Al-Laham, C.Y. Peng,
A. Nanayakkara, M. Challacombe, P.M.W. Gill, B. Johnson, W. Chen, M.W. Wong,
C. Gonzalez, J.A. Pople, Gaussian 03, Revision C.02, Gaussian, Inc., Wallingford CT, 2004.
[32] J.P. Perdew, K. Burke, Y. Wang, Phys. Rev. B 54 (1996) 16533–16539.
[33] K.D. Dobbs, W.J. Hehre, J. Comp. Chem. 8 (1987) 861–879.
[34] P.C. Hariharan, J.A. Pople, Theor. Chim. Acta 28 (1973) 213–222.
[35] J. Sebestík, S.M. Marques, P.L. Falé, S. Santos, D.M. Arduíno, S.M. Cardoso,
C.R. Oliveira, M.L. Serralheiro, M.A. Santos, J. Enz. Inhib. Med. Chem. 26 (2011) 485–497.
[36] G.L. Ellman, K.D. Courtney, V. Jr Andres, R.M. Featherstone, Biochem. Pharmacol. 7 (1961) 88–95.
[37] M. Bartolini, C. Bertucci, M.L. Bolognesi, A. Cavalli, C. Melchiorre, V. Andrisano, ChembioChem 8 (2007) 2152–2161.
[38] X. Chao, X. He, Y. Yang, X. Zhou, M. Jin, S. Liu, Z. Cheng, P. Liu, Y. Wang, J. Yu,
Y. Tan, Y. Huang, J. Qin, S. Rapposelli, Bioorg. Med. Chem. Lett. 22 (2012) 6498–6502.
[39] T. Mosmann, J. Immunol. Methods 65 (1983) 55–63.
[40] S. Chaves, A. Hiremathad, D. Tomás, R.S. Keri, L. Piemontese, M.A. Santos, New J.
Chem. 42 (2018) 16503–16515.

[41] G. Coban, L. Carlino, A.H. Tarikogullari, S. Parlar, G. Sarikaya, V. Alptuzun, A.S. Alpan, H.S. Gunes, E. Erciyas, Med. Chem. Res. 25 (2016) 2005–2014.
[42] J. Cheung, M.J. Rudolph, F. Burshteyn, M.S. Cassidy, E.N. Gary, J. Love, M.C. Franklin, J.J. Height, J. Med. Chem. 55 (2012) 10282–10286.
[43] C. Rodríguez-Rodríguez, N.S. de Groot, A. Rimola, A. Álvarez-Larena, V. Lloveras, J. Vidal-Gancedo, S. Ventura, J. Vendrell, M. Sodupe, P. González-Duarte, J. Am, Chem. Soc. 131 (2009) 1436–−1451.
[44] S. Conchinhas, MSc Thesis, IST, May, 2017.
[45] T. Leininger, A. Nicklass, H. Stoll, M. Dolg, P. Schwerdtfeger, J. Chem. Phys. 105 (1996) 1052–1059.
[46] C. Quintanova, R.S. Keri, S.M. Marques, M.G. Fernandes, S.M. Cardoso, M.L. Serralheiro, M.A. Santos, MedChemComm 6 (2015) 1969–1977.
[47] C.C. Tan, J.T. Yu, H.F. Wang, M.S. Tan, X.F. Meng, C. Wang, T. Jiang, X.C. Zhu, L. Tan, J. Alzheimers Dis. 41 (2014) 615–−631.
[48] P. Faller, C. Hureau, Dalton Trans. 7 (2009) 1080–1094.